ACS OMEGA

Open Access

http://pubs.acs.org/journal/acsodf

Article

One-Dimensional HKUST-1-Decorated Glassy Carbon Electrode for the Sensitive Electrochemical Immunosensor of NS1 Dengue Virus Serotype-3

Kariana Kusuma Dewi, Ni Luh Wulan Septiani, Shofarul Wustoni, Nugraha, Siti Nurul Aisyiyah Jenie, Robeth Viktoria Manurung, and Brian Yuliarto*

Cite This: *ACS Omega* 2024, 9, 1454−1462

Read Online

ACCESS | Metrics & More | Article Recommendations | Supporting Information

ABSTRACT: In this work, simple and sensitive detection of dengue virus serotype-3 (DENV-3) antigen was accomplished by a one-dimensional (1D) HKUST-1-functionalized electrochemical sensor. 1D HKUST-1 was synthesized via a coprecipitation method using triethanolamine (TEOA) as pH modulator and structure-directing agent. The structure, morphology, and sensing performance of the HKUST-1-decorated carbon electrode were characterized by X-ray diffraction (XRD), infrared spectroscopy (FTIR), scanning electron microscopy (SEM), cyclic voltammetry (CV), electrochemical impedance spectroscopy (EIS), and differential pulse voltammetry (DPV). We found that 40 wt% TEOA transforms the octahedron HKUST-1 to the nanorods while maintaining its crystal structure and providing chemical stability. The 1D HKUST-1-decorated carbon electrode successfully detects the antigen in the range of 0.001−10 ng/mL with a detection limit of 0.932 pg/mL. The immunosensor also exhibits remarkable performance in analyzing the antigen in human serum and showed recovery as high as ∼98% with excellent selectivity and reproducibility.

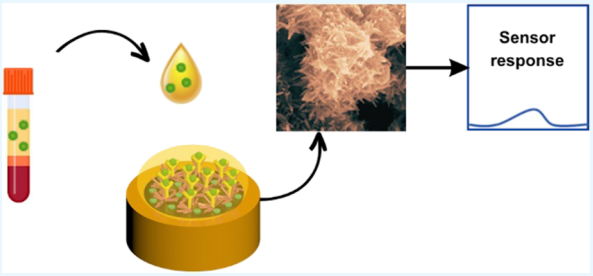

1. INTRODUCTION

The female *Aedes aegypti* mosquito spreads the dengue virus, causing outbreaks of dengue hemorrhagic fever in tropical regions. About 120 countries were affected by dengue fever, and Asia contributes 70% of the world dengue burden.[1] In 2019, 5.2 million people were infected by the dengue virus, and more than 80% are often mild, asymptomatic and have higher risk of death when not managed appropriately.[1] This virus is from the family Flaviviridae in the genus Flavivirus, which has a single-strand RNA (ssRNA) structure and a relatively small size of about 40−60 nm with a spherical shape and an isometric nucleocapsid.[2] Their mRNA contains a translation polyprotein, which is dispart by cellular proteases into three structural proteins (capsid protein C, membrane protein M, and envelope protein E), seven nonstructural proteins (NS1, NS2A, NS2B, NS3, NS4A, NS4B, and NS5), and two peptides (ER and 2k).[3] Dengue virus has four different serotypes, including DENV1, DENV2, DENV3, and DENV4.[4,5] The dengue virus serotype-3 (DENV-3) group is the most dominant vector that causes dengue hemorrhagic fever worldwide. To date, the NS1 protein is the most frequently used biomarker for the early detection of DENV-3.[6] Several studies have reported that NS1 protein released from infected cells enters the bloodstream and accumulates in blood with concentrations of up to 50 μg/mL.[5] The other reports showed that the clinical serum contains NS1 in the range of 0.04−2 μg/mL in primary DENV infection and 0.01−2 μg/mL in secondary DENV infection.[2] Moreover, dengue fever has high mortality rate with only a few effective vaccines and treatments available. The CYD-TDV (Dengvaxia) vaccine for this virus is still scarce and has many shortcomings.[7] Therefore, early detection of dengue virus infection is crucial to provide better treatment and minimize severe symptoms in patients.

The electrochemical immunosensors are reliable and highly sensitive transduction systems with low detection limits, low energy consumption, good reproducibility, high accuracy, and the capability of miniaturization and integration into small portable devices.[8,9] These features enable the development of the POC (point of care) device to diagnose the patient in real time.[10,11] In principle, the sensing event of a non-electroactive target protein can be detected by monitoring the changes in terms of capacitance or impedance properties upon interaction with the receptor unit functionalized on the sensing electrode.[10,12,13] To improve the sensing performance of electrochemical immonusensors, the integration of functional hybrid materials is the primary approach nowadays. Among the

Received: October 9, 2023
Revised: November 25, 2023
Accepted: November 30, 2023
Published: December 21, 2023

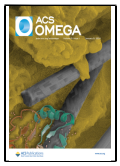

Scheme 1. Schematic Illustration of Step-by-Step Functionalization on the Carbon Electrode Surface[a]

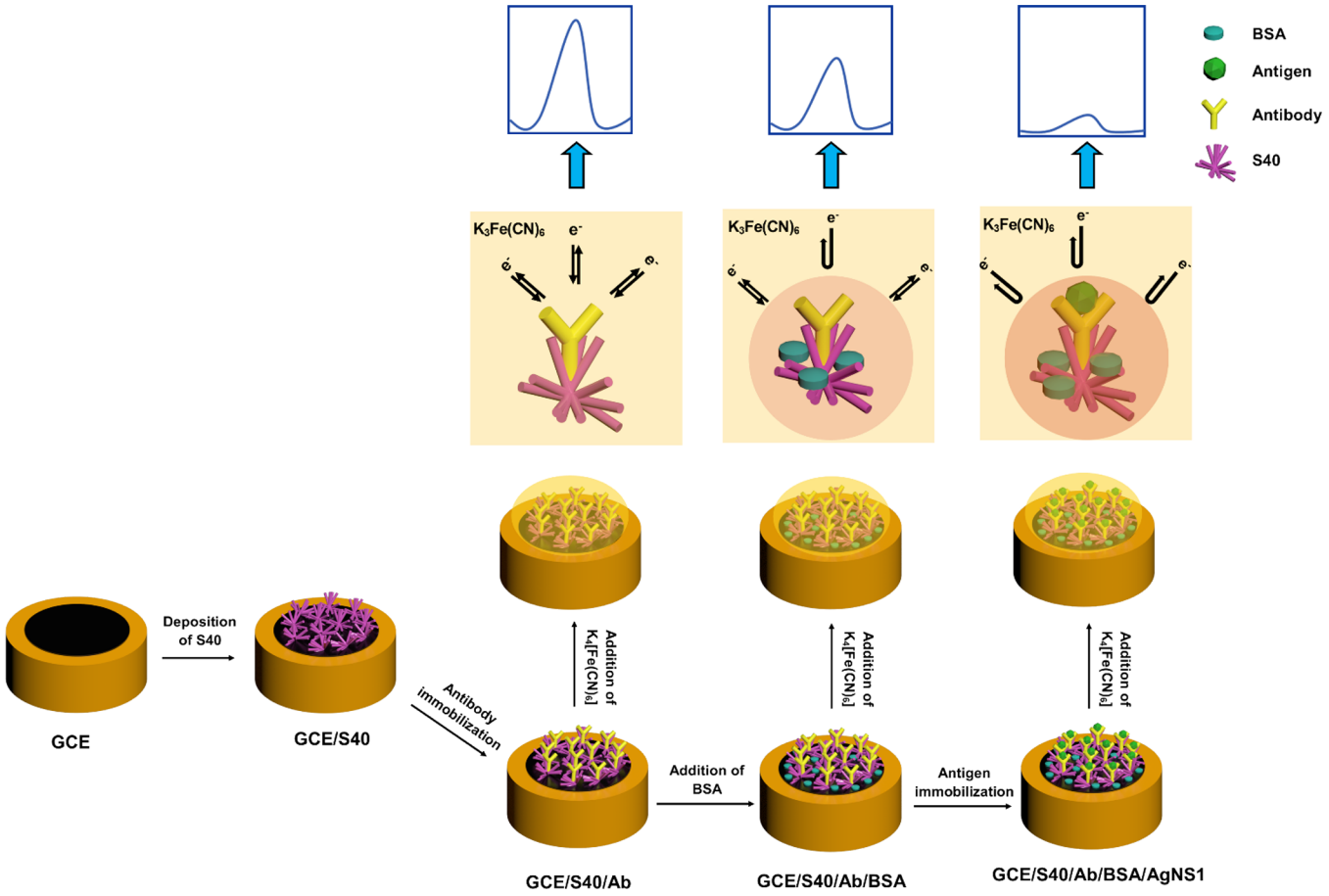

[a]The antibody-functionalized electrode surface is then used as an electrochemical immunosensor for the detection of NS1 protein biomarkers. The sensing event was quantitatively observed by monitoring the change in the redox peak using the DPV technique.

extensive library of advanced materials, metal−organic frameworks (MOFs) have been receiving tremendous attention due to their unique properties, such as a homogeneous porous crystal structure, wide-range porosity, chemical stability, and tunable functional groups on their surface.[14,15] MOF materials can be modified with terminal amine ($-NH_2$) or carboxylic (−COOH) functional groups to provide molecular immobilization sites through covalent conjugation.[16] In addition, the porous structure of MOF leads to a high electrochemical surface area, which allows a larger number of binding sites for sensing events.[17] Some works report the successfully integration of MOFs in biosensors as well as POC to detect SARS-CoV-2 nucleocapsid protein[18] and prostate cancer marker.[19,20] However, there are limited reports focusing on the development of MOF-based electrochemical sensors for specific detection of dengue virus biomarkers.

Herein, we present the systematic investigation from synthesizing HKUST-1 (Hong Kong University of Science and Technology) MOF to its application as an electrochemical sensor for NS1 protein detection. HKUST-1 is a Cu-based MOF with H_3BTC (1,3,5-benzene tricarboxylic acid) as an organic ligand. The HKUST-1 MOF has been fundamentally explored and offers diverse advantages, including biocompatibility and good electrocatalytic activity to improve the performance of the sensor system.[21] There are different strategies to modify the HKUST-1 MOF to achieve the desired properties for the specific application; for example, several types of modulators have been reported to tune the structure and control the particle size.[22−24] In this work, we demonstrate the use of triethanolamine (TEOA) as an effective modulator to form one-dimensional (1D) HKUST-1. Detailed physicochemical characterizations have been carried out to analyze the structure and morphology of modified HKUST-1. A comprehensive sensing performance of the HKUST-1-decorated carbon electrode has been performed for sensitive detection of the NS1 DENV-3 antigen.

2. EXPERIMENTAL SECTION

2.1. Materials. Dengue virus monoclonal antibody, all serotype (Anti-Dengue NS1), and dengue virus antigen (DENV-NS1 Serotype 3) (Ag ≥ 95%) were purchased from MyBiosource, USA. Copper nitrate trihydrate ($Cu(NO_3)_2$), trimesic acid (H_3BTC) with 95% of purity, Nafion, potassium ferricyanide(III) ($K_3Fe(CN)_6$) (99%), bovine serum albumin (BSA), *N*-(3-dimethylaminopropyl)-*N*′-ethylcarbodiimide hydrochloride (EDC), and *N*-hydroxy succinimide (NHS) were purchased from Sigma Aldrich, Singapore. Triethanolamine (TEOA) and ethanol (EtOH) were purchased from Merck, Singapore. Phosphate-buffered saline (PBS) was purchased from Biogear Scientific. All reagents were purchased in analytical grade and used without purification.

2.2. Synthesis of HKUST-1 MOF. HKUST-1 MOF was synthesized via the coprecipitation method at room temperature using TEOA as the modulator. The metal salt (0.05 M

https://doi.org/10.1021/acsomega.3c07856
ACS Omega 2024, 9, 1454−1462

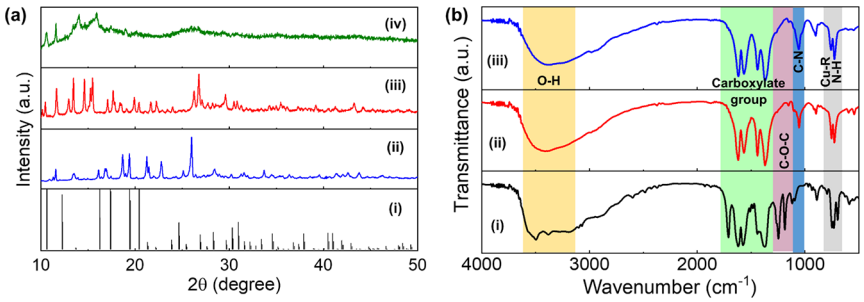

Figure 1. Characterization of modified HKUST-1 with spectroscopy techniques. (a) XRD patterns of (i) HKUST-1 from ref 25, (ii) S20, (iii) S35, and (iv) S40. (b) FTIR spectra of (i) S20, (ii) S35, and (iii) S40.

$Cu(NO_3)_2$) and organic-ligand (0.05 M trimesic acid) solutions were prepared in double-distilled water. At the same time, the modulator solution was prepared by diluting 20 wt % TEOA in water. The ligand and modulator solutions were mixed under continuous stirring until a clear solution was obtained; after that, the pH of this solution was measured. The blue color solution was formed after adding copper solution to the mixture solution in the ratio of 2:3 and followed by pH measurement. The blue precipitated product was then collected by centrifugation, washed with ethanol, and dried at 60 °C overnight. The TEOA composition was varied to 20 wt % (S20), 35 wt % (S35), and 40 wt % (S40) to evaluate the effect of the modulator on the MOF formation.

2.3. Physicochemical Characterizations of HKUST-1. Scanning electron microscopy (SEM, Hitachi SU3500, Japan) was used to characterize the morphologies of all samples. X-ray diffraction (XRD, Bruker D8 Advanced, UK) indicated the structure and investigated the new diffraction peaks. The infrared spectrum was recorded by Fourier transform infrared spectroscopy (FTIR, Shimadzu Prestige 21, Japan) to investigate the chemical bonding that formed. The specific surface area and distribution of the pore size were characterized by surface and pore analyzer (Belsorp mini, Japan). Then, a CorrTest electrochemical workstation (Wuhan CorrTest Instruments Corp., Ltd., China) was used to analyze the electrochemical characterization using cyclic voltammetry (CV), differential pulse voltammetry (DPV), and electrochemical impedance spectroscopy (EIS).

2.4. Fabrication of the HKUST-1-Decorated Carbon Electrode. The glassy carbon electrode (GCE) surface was cleaned using an alumina polishing kit, followed by sonication using ethanol and water for 5 min. Scheme 1 illustrates the electrode preparation from the bare GCE surface into the antibody-functionalized surface. HKUST-1 was dispersed in water containing 5% Nafion to obtain a homogeneous suspension (4 mg/mL). Then, 6 μL of the suspension was dropped onto the GCE surface and dried at room temperature for 5 h. Following this, the antibody was immobilized onto the GCE/HKUST-1/TEO surface and incubated at 4 °C for 16 h. Then, 3 μL of 1 wt % BSA in 0.01 M PBS was added as blocking molecules to minimize nonspecific interaction and stored at 4 °C for about 2 h. Various concentrations of NS-1 antigen DENV-3 (6 μL) were incubated onto the sensing surfaces at 4 °C overnight for the sensing measurement. After each modification, the sensing surface was washed with 0.01 M PBS to remove any unbound molecules or proteins.

2.5. Electrochemical Measurements. The electrochemical performances were investigated by CV, EIS, and DPV techniques. CV is useful for obtaining information about the redox potential and electrochemical rate of the analyte. This method measures the current generated by varying the potential based on partial cycle analysis (oxidation or reduction), one full cycle, and an assessment of the stability of the reaction products. Meanwhile, DPV is a technique that plots current variations as a potential function. Another technique commonly used is EIS. This method investigated the resistive and capacitive properties of biological disturbances that can be observed easily through the interaction of the redox reaction between the biologically mediated electrodes and the electrolyte solution. The principle of this measurement was based on the conventional three-electrode system that consists of a GCE, silver/silver chloride (Ag/AgCl), and a platinum (Pt) wire as the working electrode (modified electrode), reference electrode, and counter electrode, respectively. The CV and DPV measurement was carried out at potential ranges from 0.2 to 1.0 V in 0.01 M PBS solution containing 3 mM $K_4[Fe(CN)_6]$ with various scan rates. This electrolyte solution was also used in EIS and DPV measurements. The EIS measurement was recorded at a frequency range from 0.1 Hz to 100 kHz with an initial voltage of 0.65 V.

3. RESULTS AND DISCUSSION

3.1. Characterizations of HKUST-1-Modified TEOA. We used TEOA as a structure-directing agent and pH modulator that can control the nucleation process,[25] tuning the crystal growth, particle size, and morphology of HKUST-1. Figure 1a shows the XRD patterns of HKUST-1-modified TEOA at different concentration. The characteristic diffraction peaks of HKUST-1 generally appear at 2θ of 6.6°, 9.4°, 11.5°, and 13.3°, which represent the planes of (200), (220), (222), and (400), respectively.[26,27] The diffraction pattern of HKUST-1-modified TEOA has slight shifts in several peaks, similar to the other work on amino alcohol-modified HKUST-1.[25] In addition, 40% TEOA (S40) leads to the transformation of the crystal structure into the amorphous phase of HKUST-1, indicating the strong influence of the TEOA modulator on the formation of HKUST-1. Further, FTIR was carried out to examine the chemical bonds and composition (Figure 1b). The three samples of modified HKUST-1 with TEOA share a similar spectrum. As the common HKUST-1, they exhibit two couple bands at 1623 and 1571 cm^{-1} and 1436 and 1371 cm^{-1}, which are attributed to antisymmetry and symmetry stretching vibrations of the carboxylate group, respectively.[28−30] The bands at 1250 to 1180 cm^{-1} correspond to the C−O−C stretching vibration of H3BTC, while the band at 753 cm^{-1} is attributed to the Cu and carboxylate group coordination.[31] In addition, bands at 1052 and 721 cm^{-1} are assigned to C−N and N−H secondary amine stretching vibrations, respectively.

https://doi.org/10.1021/acsomega.3c07856
ACS Omega 2024, 9, 1454−1462

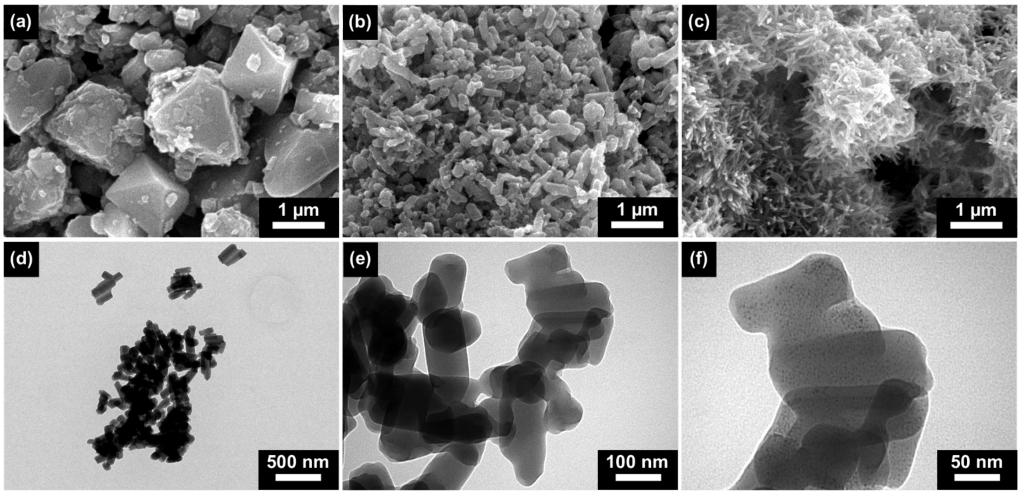

Figure 2. Characterization of HKUST-1 with electron microscopy techniques. SEM images of (a) S20, (b) S35, and (c) S40. The higher concentration of the TEOA modulator generates a nanorod-shaped structure. (d–f) TEM images of S40 with different magnifications show uniform nanorod structures.

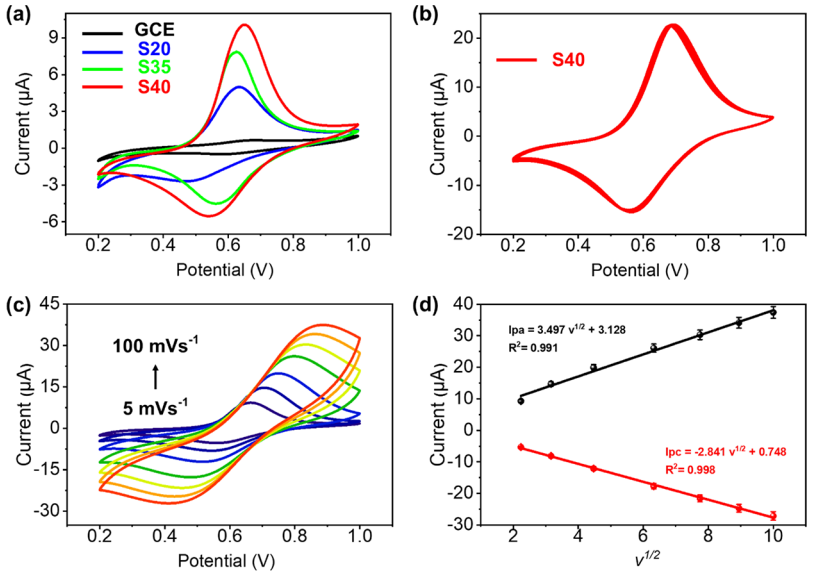

Figure 3. Electrochemical evaluation of the HKUST-1-decorated carbon electrode. (a) CV curve response of carbon electrodes with and without modification with HKUST-1. (b) Stability of the S40 electrode under a continuous CV cycle at a scan rate of 20 mV/s. (c) CV curves of the S40 electrode with different scan rates. (d) Correlation of peak current value versus square root scan rates from the S40 electrode.

These results confirm the successful formation of HKUST-1 modified with TEOA.

The morphology and nanostructure of modified HKUST-1 were characterized by using SEM and TEM, as shown in Figure 2. The SEM image of HKUST-1 with 20 wt % TEOA (S20) showed an octahedral shape (Figure 2a), which is a similar morphology of pristine HKUST-1 reported by different research groups,[27,32,33] indicating that 20 wt% TEOA does not significantly impact the HKUST-1 structure. Interestingly, a higher concentration of TEOA significantly altered the HKUST-1 morphology. We observed uniform minirods and spherical-shaped structures in the S35 sample (Figure 2b). The average diameter and length of the minirods in the S35 sample are 100 and 500 nm, respectively. Then, the HKUST-1 morphology became much smaller with the addition of 40 wt % TEOA, showing a uniform 1D nanorod structure. Whereas increasing the concentration of TEOA up to 50 wt% did not generate any MOF product, it might be due to the Cu ion tending to coordinate with TEOA, forming a Cu-TEOA complex instead of Cu-BTC MOF. This observation supports the hypothesis that TEOA plays an essential role in the synthesis process, particularly in tuning particle morphology. TEOA acts as pH modulator and structure-directing agent, which change the pH of the reaction environment during MOF formation. As shown in Table S1, it is confirmed that a higher concentration of TEOA induces an increase in the pH of the reagent solution. It is known that a higher pH can accelerate the nucleation rate because more H_3BTC are deprotonated, providing higher coordination sites with metal ions (Cu^{2+}). This phenomenon can yield smaller particle sizes.[34] We then further confirm the formation of the 1D nanorod structure of the S40 sample using TEM. The TEM images of the S40 sample are displayed in Figure 2d–f, and the average sizes of diameter and length are 45 and 100 nm, respectively, in line with the SEM results. These results confirmed that adding TEOA successfully controls the

https://doi.org/10.1021/acsomega.3c07856
ACS Omega 2024, 9, 1454–1462

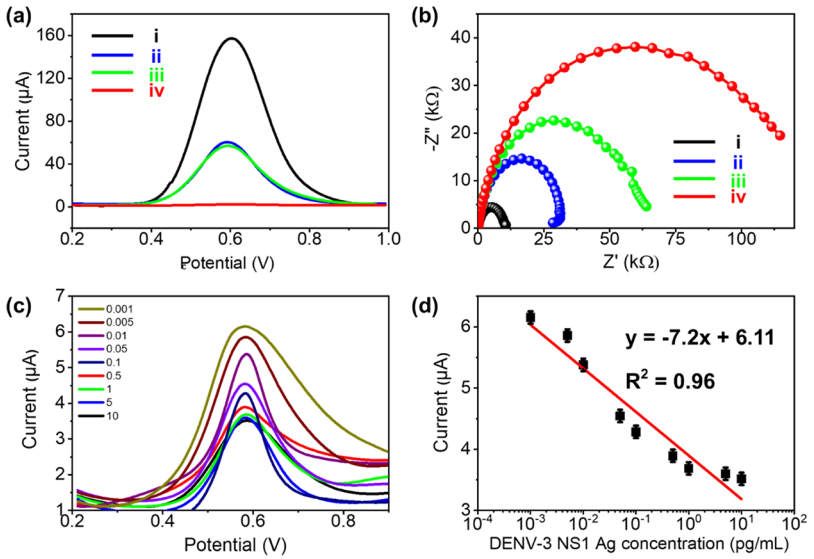

Figure 4. Electrochemical measurement of the S40 electrodes. (a) DPV curves of (i) GCE/S40, (ii) GCE/S40/Ab, (iii) GCE/S40/Ab/BSA, and (iv) GCE/S40/Ab/BSA/AgNS1. (b) Nyquist plots of (i) GCE/S40, (ii) GCE/S40/Ab, (iii) GCE/S40/Ab/BSA, and (iv) GCE/S40/Ab/BSA/AgNS1. Ab stands for antibody, BSA is bovine serum albumin, and AgNS1 is NS1 antigen. (c) DPV curves of antibody-modified S40 electrodes after incubation with different concentrations of NS1 antigen: from top to bottom, 0.001, 0.005, 0.01, 0.05, 0.1, 0.5, 1, 5, and 10 ng/mL. (d) Calibration plot of the immunosensor with linear regression: $y = -0.72x + 6.11$ and $R^2 = 0.96$.

morphology of HKUST-1, which can generate homogeneous particle distribution.

The N_2 adsorption/desorption isotherm curve of all modified HKUST-1 samples is shown in Figure S1. Brunauer-Emmet-Teller (BET) calculation was carried out to obtain specific surface area. Based on the BET calculation, the specific surface areas of S20, S35, and S40 are 1762, 694, and 703 m^2/g, respectively, with the average pore volumes of 1.61, 0.65, and 0.93 cm^3/g, respectively. In this case, S20 exhibits the highest surface area compared to the S40 sample relating to its high pore volume. The lower surface area of S40 might be due to the presence of TEOA or Cu-TEOA complex that affects the porosity of HKUST-1. This study is comparable to other reports, in which the nanocrystals have lower surface area and pore volume than bulk crystal and the hierarchical octahedral-shaped crystal has a specific surface area of 993.6 m^2/g and a pore volume 0.47 cm^3/g.[35]

3.2. Electrochemical Evaluation of the HKUST-1-Decorated Carbon Electrode. We first evaluated the electrochemical performance of carbon electrodes before and after modification with HKUST-1 using CV in 0.01 M PBS containing 3 mM $K_4[Fe(CN)_6]$ at a scan rate of 5 mV/s. Figure 3a shows the comparison of the CV curves from the samples, showing that the addition of HKUST-1 improves the electrocatalytic properties of the electrode. Taking into account the similar amount of modified HKUST-1 decorated on carbon electrodes with identical geometry, the S40 electrode exhibited the highest redox peak. We suggested that this superior performance could be related to the homogeneous 1D nanorod structure of HKUST-1 S40. Such morphology could provide a larger active surface area, leading to higher capacitance and lower electron transfer resistance. Therefore, we selected S40 as the best-performing material and explored it further as the matrix of the electrochemical immunosensors for NS1 DENV-3 detection. Furthermore, Figure 3b shows the good stability of the S40 electrode under continuous CV cycles at a scan rate of 20 mV/s. Figure 3c displays the CV of the S40 electrode at different scan rates. The increasing scan rate corresponds to the rising current and redox peaks with an excellent linear relationship ($R^2 = 0.99$), indicating that the reaction process is mainly by diffusion. In addition, these CV profiles can be used to estimate the effective surface area (ESA) using the Randles−Sevcik equation (eq 1),

$$i_{pa} = 0.4463nFAC\left(\frac{nFvD}{RT}\right)^{1/2} = 2.69 \times 10^5 n^{3/2} ACD^{1/2} v^{1/2} \text{ at } 25\ ^\circ\text{C} \quad (1)$$

where i_{pa} (A) is the current peak in the oxidation process, n is the total number of electrons exchanged in a redox reaction, in this case, equal to 1, A (cm^2) is the effective surface area (ESA), C (mol cm^{-3}) is the concentration of the molecule $Fe(CN)_6]^{3-}$ in the solution (0.003 M), D ($cm^2\ s^{-1}$) is the diffusion coefficient of $Fe(CN)_6]^{3-}$ (6.5×10^{-6} $cm^2\ s^{-1}$), and v ($V\ s^{-1}$) is the scan rate. Based on the peak current value versus the square root of scan rates in Figure 3d, the calculated slope is 3.497. Hence, the ESA of the S40 electrode is estimated at *ca.* 1.6997 cm^2. The HKUST-1-decorated carbon electrode in this work showed a superior value compared to other works that reported that the active surface areas of the bare GCE and activated GCE were 0.11 and 0.58 cm^2, respectively, even in 5 mM $Fe(CN)_6]^{3-}$.[36]

3.3. Detection of NS-1 Dengue Virus Serotype 3 (DENV-3). The sensing performance of the S40 electrode for detecting NS1 DENV-3 protein was assessed using the DPV technique. The DPV technique is powerful for analyzing the Faradaic current generated by the redox reaction at the electrode−electrolyte interface while minimizing the charging effect from the electrical double layer.[37] Figure 4a shows the evolution of the DPV curve after the step-by-step modification on the S40 electrode. GCE/S40 possesses a relatively high current response compared to the bare GCE, showing the high conductivity of S40 as reflected in Figure 3a. The 1D structure of S40 allows better electronic properties that highly contribute to the electrochemical biosensor performance. The current

https://doi.org/10.1021/acsomega.3c07856
ACS Omega 2024, 9, 1454−1462

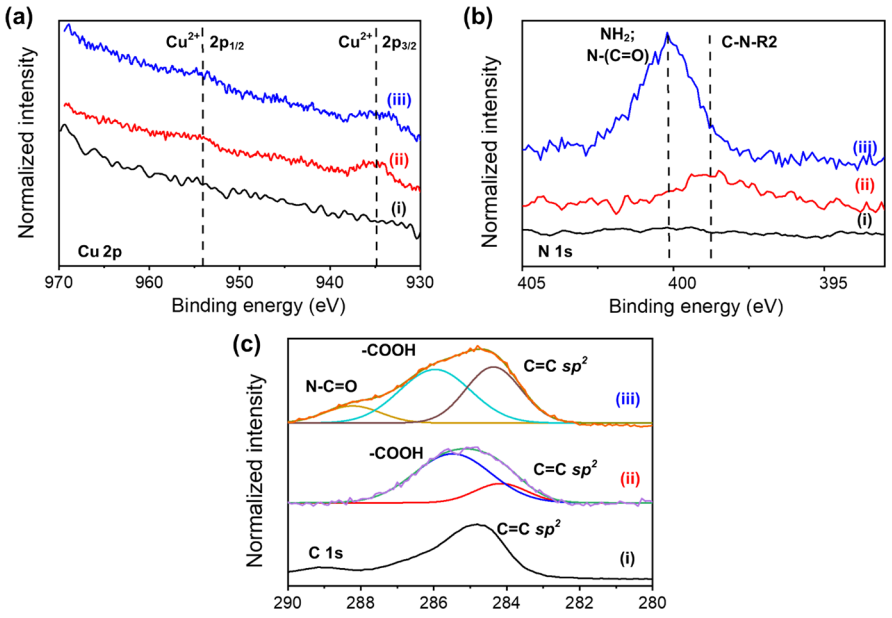

Figure 5. High-resolution XPS of SPCE (i), SPCE/S40 (ii), and SPCE/S40/Ab (iii) in the regions of (a) Cu 2p, (b) N 1s, and (c) C 1s.

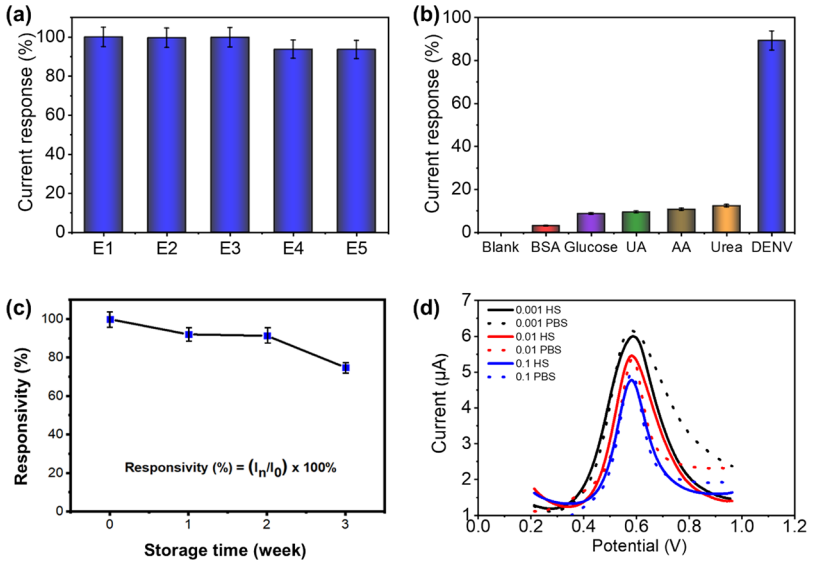

Figure 6. Sensing performance of the immunosensors. (a) Reproducibility of five immunosensors (E1−E5) for detecting 10 ng/mL NS1 antigen in a typical procedure. (b) Selectivity of the immunosensor after incubation with different biomolecules: bovine serum albumin (BSA), glucose, uric acid (UA), ascorbic acid (AA), urea, and the specific antigen NS1. (c) Stability of the immunosensors during storage. (d) Detection of the immunosensor with a variation of concentrations of 0.001 ng/mL (yellow), 0.01 ng/mL (blue), and 0.1 ng/mL (red) NS1 antigen in clinical human serum (dashed line) and 0.01 M PBS (solid line).

peak decreases significantly upon introducing antibodies with an incubation time of 16 h (Figure S2), representing the higher resistance of the electron transfer process between the redox probe and the electrode due to the intrinsic nature of insulating properties from the immobilized antibodies.[38] High-resolution XPS was carried out to prove the occurrence of a binding event of the antibody on the surface of the S40 electrode (Figure 5). In this case, a screen-printed carbon electrode (SPCE) was used as a working electrode. The S40 sample was deposited on the surface of SPCE and modified using a similar procedure. Cu^{2+} 2p was observed in the binding energy region of 915−975 eV as seen in Figure 5a. Peaks at 934.8 and 954.0 observed in SPCE/S40 and SPCE/S40/Ab originate from Cu^{2+} $2p_{3/2}$ and $2p_{1/2}$, respectively.[39,40] The Cu^{2+} peak intensity of SPCE/S40/Ab appears to be smaller than that of SPCE/S40, indicating the presence of other molecules on the surface of the electrode. In addition, those peaks do not appear in the bare SPCE. Also, the attachment of antibody on the surface of S40 was proven by the existence of the peak of amine that originated from the antibody protein at a binding energy of 400.2 eV in the N 1s region as seen in Figure 5b.[41,42] Moreover, a small peak at 398.8 eV in the SPCE/S40 sample also comes from amine species that originated from the interaction between S40 and triethanolamine. Furthermore, the C 1s spectrum was observed in the region of 280−290 eV as seen in Figure 5c. Carbon sp^2 is represented by the peak at 284.2 and 284.8 eV in bare SPCE and modified SPCE, respectively.[43,44] The binding event between S40 and antibody

https://doi.org/10.1021/acsomega.3c07856
ACS Omega 2024, 9, 1454−1462

is marked by the peak at binding energies of 286.07 and 288.27 eV, which are attributed to the carboxyl group of −COOH and the amide bond of N−C═O.[45,46] The addition of BSA, which serves as a blocking protein to minimize nonspecific interaction,[47] slightly reduced the peak, indicating that the sensing surface was covered mainly by the high-density immobilized antibody.

The addition of target NS1 protein notably reduces the peak further, showing a negligible faradaic current. The decreasing current in the DPV curves corresponds to the addition of nonconductive molecules onto the electrode, indicating the successful binding between the target NS-1 DENV-3 antigen and antibodies that further hinder the redox probe ion from reaching the sensing surface. Furthermore, EIS measurement was carried out to quantitatively examine the change in charge transfer resistance (R_{ct}) during functionalization and sensing processes. R_{ct} is a helpful parameter extracted from the fitting of the Nyquist plot for studying the modifications on the electrode surface and has been widely used as a sensing signal in electrochemical immunosensors.[48−50] The Nyquist plot of S40 electrodes before and after surface modification is shown in Figure 4b. The R_{ct} of the S40 electrode is about 10 kΩ (curve i). The R_{ct} value gradually increased to 30 kΩ (curve ii), 60 kΩ (curve iii), and 110 kΩ (curve iv) after incubation of the DENV monoclonal antibody, BSA, and NS1 DENV-1 antigen, respectively. The EIS results support the trends in the DPV curves representing the presence of the antibody and BSA and the interaction of antigen to the sensing surface.

3.4. Sensitivity of the Immunosensor. Figure 4c shows the DPV curves obtained after incubating the antibody-modified S40 electrodes with different concentrations of NS1 DENV-3 antigen from 0.001 to 10 ng/mL. The peak current was directly related to the number of antigens captured on the sensing surface. The decreasing current corresponds to higher antigen proteins adsorbed on the sensing surface. A calibration curve between the peak current versus the concentration of the NS1 DENV-3 antigen is shown in Figure 4b. The limit of detection (LOD) can be defined as the smallest concentration detected by the immunosensors, generally obtained using the equation LOD = $3s/b$ (where s is the standard deviation of the intercept, and b is the slope of the calibration curve).[15,51] We calculate the LOD of the immunosensors around 0.932 pg/mL with 96% linearity. These results are superior compared to the other reported works in Table S2.

3.5. Reproducibility and Selectivity. To further assess the quality of the immunosensors, we first demonstrated the reproducibility test using five different sensors incubated with 10 ng/mL antigen and measured the DPV curves. Figure 6a shows almost identical responses, indicating the excellent reproducibility of the sensing electrodes. We also examined the selectivity of the immunosensor by exposing the sensing surface to different nonspecific targets such as bovine serum albumin (BSA), glucose, uric acid (UA), ascorbic acid (AA), and urea using the concentration of 10 ng/mL in 0.01 M PBS and incubated in a similar way to the sensing measurement. The results are analyzed by eq 2, where I_0 is the baseline signal obtained after antibody immobilization, and I_n is the response signal after incubation with the biomolecules. Figure 6b shows the sensing response after the incubation with different biomolecules. The nonspecific biomolecules only generated a minimal response (3−12%) compared to the signal generated after incubation with NS1 antigen (89%), indicating the excellent specificity of the immunosensors to detect the NS1 antigen.

$$\Delta I_n = \frac{(I_0 - I_n)}{I_0} \times 100\% \quad (2)$$

3.6. Stability of the Immunosensor. To assess the stability of the immunosensor, the sensor was repeatedly measured for three weeks under storage at 4 °C. The responsivity (Figure 6c) was calculated by dividing the peak oxidation current at a particular week (I_n) with the initial peak oxidation current (I_0). After 2 weeks, the responsivity was approximately 92% compared to the initial responsivity and decreased to 75% after 3 weeks. The decline in the responsiveness of the immunosensor is probably due to changes in active antibodies and the presence of residues attached to the surface during repeated measurements. This observation indicated that the immunosensor-based modified HKUST-1 with 40 wt % TEOA has good stability in a long lifespan of about 2 weeks.

3.7. Clinical Detection in Human Serum. A further experiment was performed in human serum to evaluate the potential clinical applications of the immunosensor. Three immunosensors were prepared under the same conditions to detect three variations of NS1 antigen DENV-3 concentrations in normal human serum, diluted 100× in PBS solution. Figure 6d shows the results for detecting 0.001, 0.01, and 0.1 ng/mL NS1 antigen DENV-3 in human serum compared to the sensing results in PBS. The recoveries of the three samples are 97.52, 101.45, and 96%, respectively (Table 1). This test shows that the immunosensors could detect the target in complex media and have the potential for further development toward point-of-care technology.

Table 1. Recovery of Antigen Detection in Human Serum

sample	spiked (ng/mL)	found (ng/mL)	recovery (%)
a	0.001	0.000975	97.52
b	0.01	0.010145	101.45
c	0.1	0.096011	96.01

4. CONCLUSIONS

In summary, 1D HKUST-1 was successfully synthesized using the coprecipitation method by utilizing TEOA as a modulator and structure-directing agent. The concentration of TEOA strongly affects the morphology of HKUST-1. TEOA (40 wt %) produces highly uniform nanorod HKUST-1 (S40). The S40-decorated carbon electrode exhibits the best performance in terms of their electrochemical properties. The antibody-modified S40 electrode shows high sensitivity to NS1 DENV-3 antigen in the linear range of 0.001−10 ng/mL with a detection limit of 0.932 pg/mL. Moreover, the proposed electrochemical immunosensors demonstrate cheap and easy fabrication of electrode, considerable reproducibility, excellent specificity, good stability under continuous CV cycles, and operational stability over 2 weeks. The decreased performance after 2 weeks of storage limits 1D HKUST-1 was observed in long-term operation; therefore, further study needs to be carried out. However, this work could provide insights for further integration of advanced materials such as MOFs with electrochemical devices for point-of-care technology.

https://doi.org/10.1021/acsomega.3c07856
ACS Omega 2024, 9, 1454−1462

■ ASSOCIATED CONTENT

Supporting Information

The Supporting Information is available free of charge at https://pubs.acs.org/doi/10.1021/acsomega.3c07856.

pH value of the reagent solution with the addition of TEOA, N_2 adsorption desorption curve, effect of antibody incubation time to the current response of the GCE/S40/Ab electrode, and comparison of the electrochemical immunosensor for dengue virus detection (PDF)

■ AUTHOR INFORMATION

Corresponding Author

Brian Yuliarto − *Advanced Functional Materials Laboratory, Faculty of Industrial Technology, BRIN and ITB Collaboration Research Center for Biosensor and Biodevices, and Research Center for Nanoscience and Nanotechnology (RCNN), Institut Teknologi Bandung, Bandung 40132, Indonesia;* orcid.org/0000-0003-0662-7923; Email: brian@itb.ac.id

Authors

Kariana Kusuma Dewi − *Advanced Functional Materials Laboratory, Faculty of Industrial Technology and BRIN and ITB Collaboration Research Center for Biosensor and Biodevices, Institut Teknologi Bandung, Bandung 40132, Indonesia*

Ni Luh Wulan Septiani − *Advanced Functional Materials Laboratory, Faculty of Industrial Technology and BRIN and ITB Collaboration Research Center for Biosensor and Biodevices, Institut Teknologi Bandung, Bandung 40132, Indonesia; Research Center for Advanced Materials, National Research and Innovation Agency (BRIN), South Tangerang, Banten 15314, Indonesia*

Shofarul Wustoni − *Biological and Environmental Science and Engineering Division (BESE), King Abdullah University of Science and Technology (KAUST), Thuwal 23955-6900, Saudi Arabia*

Nugraha − *Advanced Functional Materials Laboratory, Faculty of Industrial Technology and Research Center for Nanoscience and Nanotechnology (RCNN), Institut Teknologi Bandung, Bandung 40132, Indonesia*

Siti Nurul Aisyiyah Jenie − *BRIN and ITB Collaboration Research Center for Biosensor and Biodevices, Institut Teknologi Bandung, Bandung 40132, Indonesia; Research Center for Chemistry, National Research and Innovation Agency (BRIN), Tangerang Selatan, Banten 15314, Indonesia*

Robeth Viktoria Manurung − *BRIN and ITB Collaboration Research Center for Biosensor and Biodevices, Institut Teknologi Bandung, Bandung 40132, Indonesia; Research Centre for Electronics, National Research and Innovation Agency (BRIN), Bandung, Jawa Barat 40135, Indonesia*

Complete contact information is available at: https://pubs.acs.org/10.1021/acsomega.3c07856

Notes

The authors declare no competing financial interest.

■ ACKNOWLEDGMENTS

This work is financially supported by Institut Teknologi Bandung under the grant scheme of Riset Unggulan (No. FTI.PN-6-16-2023) . B.Y. acknowledges financial support from National Research and Innovation Agency under the grant scheme of Research Collaboration Center.

■ REFERENCES

(1) Srisawat, N.; Thisyakorn, U.; Ismail, Z.; Rafiq, K.; Gubler, D. J.; Clapham, H. E. Committee, on behalf of A.-I. W. D. D. World Dengue Day: A Call for Action. *PLoS Negl. Trop. Dis.* **2022**, *16* (8), No. e0010586-.

(2) Kim, J. H.; Cho, C. H.; Ryu, M. Y.; Kim, J. G.; Lee, S. J.; Park, T. J.; Park, J. P.; D'Auria, S. Development of Peptide Biosensor for the Detection of Dengue Fever Biomarker, Nonstructural 1. *PLoS One* **2019**, *1* (9), No. e0222144-.

(3) Nasar, S.; Rashid, N.; Iftikhar, S. Dengue Proteins with Their Role in Pathogenesis, and Strategies for Developing an Effective Anti-Dengue Treatment: A Review. *J Med Virol* **2020**, *92* (8), 941−955.

(4) Meng, F.; Badierah, R. A.; Almehdar, H. A.; Redwan, E. M.; Kurgan, L.; Uversky, V. N. Unstructural Biology of the Dengue Virus Proteins. *FEBS J* **2015**, *282* (17), 3368−3394.

(5) Lim, J. M.; Kim, J. H.; Ryu, M. Y.; Cho, C. H.; Park, T. J.; Park, J. P. An Electrochemical Peptide Sensor for Detection of Dengue Fever Biomarker NS1. *Anal. Chim. Acta* **2018**, *1026*, 109−116.

(6) Cecchetto, J.; Santos, A.; Mondini, A.; Cilli, E. M.; Bueno, P. R. Serological Point-of-Care and Label-Free Capacitive Diagnosis of Dengue Virus Infection. *Biosens Bioelectron* **2020**, *151*, No. 111972.

(7) Jin, S.-A.; Poudyal, S.; Marinero, E. E.; Kuhn, R. J.; Stanciu, L. A. Impedimetric Dengue Biosensor Based on Functionalized Graphene Oxide Wrapped Silica Particles. *Electrochim. Acta* **2016**, *194*, 422−430.

(8) Zheng, Y.; Li, J.; Zhou, B.; Ian, H.; Shao, H. Advanced Sensitivity Amplification Strategies for Voltammetric Immunosensors of Tumor Marker: State of the Art. *Biosens Bioelectron* **2021**, *178*, No. 113021.

(9) Lv, S.; Zhang, K.; Zhu, L.; Tang, D.; Niessner, R.; Knopp, D. H2-Based Electrochemical Biosensor with Pd Nanowires@ZIF-67 Molecular Sieve Bilayered Sensing Interface for Immunoassay. *Anal. Chem.* **2019**, *91* (18), 12055−12062.

(10) Goud, K. Y.; Reddy, K. K.; Khorshed, A.; Kumar, V. S.; Mishra, R. K.; Oraby, M.; Ibrahim, A. H.; Kim, H.; Gobi, K. V. Electrochemical Diagnostics of Infectious Viral Diseases: Trends and Challenges. *Biosens Bioelectron* **2021**, *180*, No. 113112.

(11) Tepeli, Y.; Ülkü, A. Electrochemical Biosensors for Influenza Virus a Detection: The Potential of Adaptation of These Devices to POC Systems. *Sens Actuators B Chem* **2018**, *254*, 377−384.

(12) Zhang, J.-X.; Lv, C.-L.; Tang, C.; Wang, A.-J.; Mei, L.-P.; Song, P.; Feng, J.-J. Sandwich-Type Ultrasensitive Immunosensing of Breast Cancer Biomarker Based on Core-Shell Au@PdAg Dog-Bone-like Nanostructures and Au@PtRh Nanorods. *Sens Actuators B Chem* **2023**, *382*, No. 133497.

(13) Mao, Y.-W.; Zhang, J.-X.; Chen, D.-N.; Wang, A.-J.; Feng, J.-J. Bimetallic PtFe Alloyed Nanoparticles Decorated on 3D Hollow N-Doped Carbon Nanoflowers as Efficient Electrochemical Biosensing Interfaces for Ultrasensitive Detection of SCCA. *Sens Actuators B Chem* **2022**, *370*, No. 132416.

(14) Mohan, B.; Kumar, S.; Xi, H.; Ma, S.; Tao, Z.; Xing, T.; You, H.; Zhang, Y.; Ren, P. Fabricated Metal-Organic Frameworks (MOFs) as Luminescent and Electrochemical Biosensors for Cancer Biomarkers Detection. *Biosens Bioelectron* **2022**, *197*, No. 113738.

(15) Gao, Y.; Li, M.; Zeng, Y.; Liu, X.; Tang, D. Tunable Competitive Absorption-Induced Signal-On Photoelectrochemical Immunoassay for Cardiac Troponin I Based on Z-Scheme Metal−Organic Framework Heterojunctions. *Anal. Chem.* **2022**, *94* (39), 13582−13589.

(16) Zhang, S.; Rong, F.; Guo, C.; Duan, F.; He, L.; Wang, M.; Zhang, Z.; Kang, M.; Du, M. Metal−Organic Frameworks (MOFs) Based Electrochemical Biosensors for Early Cancer Diagnosis in Vitro. *Coord. Chem. Rev.* **2021**, *439*, No. 213948.

(17) Wang, Y.; Hu, Y.; He, Q.; Yan, J.; Xiong, H.; Wen, N.; Cai, S.; Peng, D.; Liu, Y.; Liu, Z. Metal-Organic Frameworks for Virus Detection. *Biosens Bioelectron* **2020**, *169*, No. 112604.
(18) Zeng, R.; Qiu, M.; Wan, Q.; Huang, Z.; Liu, X.; Tang, D.; Knopp, D. Smartphone-Based Electrochemical Immunoassay for Point-of-Care Detection of SARS-CoV-2 Nucleocapsid Protein. *Anal. Chem.* **2022**, *94* (43), 15155−15161.
(19) Yu, Z.; Tang, J.; Gong, H.; Gao, Y.; Zeng, Y.; Tang, D.; Liu, X. Enzyme-Encapsulated Protein Trap Engineered Metal−Organic Framework-Derived Biomineral Probes for Non-Invasive Prostate Cancer Surveillance. *Adv Funct Mater* **2023**, *33* (26), 2301457.
(20) Chen, Y.; Yuan, P.-X.; Wang, A.-J.; Luo, X.; Xue, Y.; Zhang, L.; Feng, J.-J. A Novel Electrochemical Immunosensor for Highly Sensitive Detection of Prostate-Specific Antigen Using 3D Open-Structured PtCu Nanoframes for Signal Amplification. *Biosens Bioelectron* **2019**, *126*, 187−192.
(21) Liu, X.; Yue, T.; Qi, K.; Qiu, Y.; Guo, X. Porous Graphene Based Electrochemical Immunosensor Using Cu(3)(BTC)(2) Metal-Organic Framework as Nonenzymatic Label. *Talanta* **2020**, *217*, No. 121042.
(22) Mu, X.; Chen, Y.; Lester, E.; Wu, T. Optimized Synthesis of Nano-Scale High Quality HKUST-1 under Mild Conditions and Its Application in CO2 Capture. *Microporous Mesoporous Mater.* **2018**, *270*, 249−257.
(23) Xin, C.; Zhan, H.; Huang, X.; Li, H.; Zhao, N.; Xiao, F.; Wei, W.; Sun, Y. Effect of Various Alkaline Agents on the Size and Morphology of Nano-Sized HKUST-1 for CO2 Adsorption. *RSC Adv* **2015**, *5* (35), 27901−27911.
(24) Kubo, M.; Saito, T.; Shimada, M. Evaluation of the Parameters Utilized for the Aerosol-Assisted Synthesis of HKUST-1. *Microporous Mesoporous Mater.* **2017**, *245*, 126−132.
(25) Manos, M. J.; Moushi, E. E.; Papaefstathiou, G. S.; Tasiopoulos, A. J. New Zn2+ Metal Organic Frameworks with Unique Network Topologies from the Combination of Trimesic Acid and Amino-Alcohols. *Cryst Growth Des* **2012**, *12* (11), 5471−5480.
(26) Zhou, L.; Niu, Z.; Jin, X.; Tang, L.; Zhu, L. Effect of Lithium Doping on the Structures and CO2 Adsorption Properties of Metal-Organic Frameworks HKUST-1. *ChemistrySelect* **2018**, *3* (45), 12865−12870.
(27) Denning, S.; Majid, A. A. A.; Lucero, J. M.; Crawford, J. M.; Carreon, M. A.; Koh, C. A. Metal−Organic Framework HKUST-1 Promotes Methane Hydrate Formation for Improved Gas Storage Capacity. *ACS Appl Mater Interfaces* **2020**, *12* (47), 53510−53518.
(28) Dewi, K. K.; Septiani, N. L. W.; Nugraha, N.; Natalia, D.; Yuliarto, B. Amorphous HKUST-1 Nanoparticles and Their Modification for Highly Sensitive Dengue Virus Immunosensor. *J. Electrochem. Soc.* **2022**, *169* (9), No. 097506.
(29) Sun, X.; Gu, X.; Xu, W.; Chen, W. J.; Xia, Q.; Pan, X.; Zhao, X.; Li, Y.; Wu, Q. H. Novel Hierarchical Fe(III)-Doped Cu-MOFs With Enhanced Adsorption of Benzene Vapor. *Front. Chem.* **2019**, 652.
(30) Zhu, C.; Zhang, Z.; Wang, B.; Chen, Y.; Wang, H.; Chen, X.; Zhang, H.; Sun, N.; Wei, W.; Sun, Y. Synthesis of HKUST-1#MCF Compositing Materials for CO2 Adsorption. *Microporous Mesoporous Mater.* **2016**, *226*, 476−481.
(31) Lu, H.; Zhang, L.; Wang, B.; Long, Y.; Zhang, M.; Ma, J.; Khan, A.; Chowdhury, S. P.; Zhou, X.; Ni, Y. Cellulose-Supported Magnetic Fe3O4−MOF Composites for Enhanced Dye Removal Application. *Cellulose* **2019**, *26* (8), 4909−4920.
(32) Dubale, A. A.; Ahmed, I. N.; Chen, X.-H.; Ding, C.; Hou, G.-H.; Guan, R.-F.; Meng, X.; Yang, X.-L.; Xie, M.-H. A Highly Stable Metal−Organic Framework Derived Phosphorus Doped Carbon/Cu2O Structure for Efficient Photocatalytic Phenol Degradation and Hydrogen Production. *J Mater Chem A Mater* **2019**, *7* (11), 6062−6079.
(33) Liu, Q.; Yang, J.-M.; Jin, L.-N.; Sun, W.-Y. Metal Ion Induced Porous HKUST-1 Nano/Microcrystals with Controllable Morphology and Size. *CrystEngComm* **2016**, *18* (22), 4127−4132.
(34) Tovar, T. M.; Zhao, J.; Nunn, W. T.; Barton, H. F.; Peterson, G. W.; Parsons, G. N.; LeVan, M. D. Diffusion of CO2 in Large Crystals of Cu-BTC MOF. *J. Am. Chem. Soc.* **2016**, *138* (36), 11449−11452.
(35) Wang, F.; Guo, H.; Chai, Y.; Li, Y.; Liu, C. The Controlled Regulation of Morphology and Size of HKUST-1 by "Coordination Modulation Method.". *Microporous Mesoporous Mater.* **2013**, *173*, 181−188.
(36) Murugan, P.; Nagarajan, R. D.; Sundramoorthy, A. K.; Ganapathy, D.; Atchudan, R.; Nallaswamy, D.; Khosla, A. Electrochemical Detection of H2O2 Using an Activated Glassy Carbon Electrode. *ECS Sensors Plus* **2022**, *1* (3), No. 034401.
(37) Palomar, Q.; Xu, X. X.; Gondran, C.; Holzinger, M.; Cosnier, S.; Zhang, Z. Voltammetric Sensing of Recombinant Viral Dengue Virus 2 NS1 Based on Au Nanoparticle−Decorated Multiwalled Carbon Nanotube Composites. *Microchimica Acta* **2020**, *187* (6), 1−10.
(38) Figueiredo, A.; Vieira, N. C. S.; Dos Santos, J. F.; Janegitz, B. C.; Aoki, S. M.; Junior, P. P.; Lovato, R. L.; Nogueira, M. L.; Zucolotto, V.; Guimarães, F. E. G.Electrical Detection of Dengue Biomarker Using Egg Yolk Immunoglobulin as the Biological Recognition Element. *Sci Rep***2015**, *5*. DOI: 10.1038/srep07865.
(39) Stawowy, M.; Jagódka, P.; Matus, K.; Samojeden, B.; Silvestre-Albero, J.; Trawczyński, J.; Łamacz, A.HKUST-1-Supported Cerium Catalysts for CO Oxidation. *Catalysts***2020**, *10* (1). 108.
(40) Domán, A.; Nagy, B.; Nichele, L. P.; Srankó, D.; Madarász, J.; László, K. Pressure Resistance of Copper Benzene-1,3,5-Tricarboxylate − Carbon Aerogel Composites. *Appl. Surf. Sci.* **2018**, *434*, 1300−1310.
(41) Ederer, J.; Janoš, P.; Ecorchard, P.; Tolasz, J.; Štengl, V.; Beneš, H.; Perchacz, M.; Pop-Georgievski, O. Determination of Amino Groups on Functionalized Graphene Oxide for Polyurethane Nanomaterials: XPS Quantitation vs. *Functional Speciation. RSC Adv* **2017**, *7* (21), 12464−12473.
(42) Linh, N. D.; Huyen, N. T. T.; Dang, N. H.; Piro, B.; Thi Thu, V. Electrochemical Interface Based on Polydopamine and Gold Nanoparticles/Reduced Graphene Oxide for Impedimetric Detection of Lung Cancer Cells. *RSC Adv* **2023**, *13* (15), 10082−10089.
(43) Zubair, U.; Amici, J.; Crespiera, S. M.; Francia, C.; Bodoardo, S. Rational Design of Porous Carbon Matrices to Enable Efficient Lithiated Silicon Sulfur Full Cell. *Carbon N Y* **2019**, *145*, 100−111.
(44) Lesiak, B.; Kövér, L.; Tóth, J.; Zemek, J.; Jiricek, P.; Kromka, A.; Rangam, N. C Sp2/Sp3 Hybridisations in Carbon Nanomaterials − XPS and (X)AES Study. *Appl. Surf. Sci.* **2018**, *452*, 223−231.
(45) Gong, X.; Bi, Y.; Zhao, Y.; Liu, G.; Teoh, W. Y. Graphene Oxide-Based Electrochemical Sensor: A Platform for Ultrasensitive Detection of Heavy Metal Ions. *RSC Adv* **2014**, *4* (47), 24653−24657.
(46) Adesina, A.; Mashazi, P.Oriented Antibody Covalent Immobilization for Label-Free Impedimetric Detection of C-Reactive Protein via Direct and Sandwich Immunoassays. *Front Chem***2021**, *9*.
(47) Kim, J. H.; Cho, C. H.; Ryu, M. Y.; Kim, J.-G.; Lee, S.-J.; Park, T. J.; Park, J. P. Development of Peptide Biosensor for the Detection of Dengue Fever Biomarker, Nonstructural 1. *PLoS One* **2019**, *14* (9), No. e0222144.
(48) Singh, N.; Nayak, J.; Patel, K.; Sahoo, S. K.; Kumar, R. Electrochemical Impedance Spectroscopy Reveals a New Mechanism Based on Competitive Binding between Tris and Protein on a Conductive Biomimetic Polydopamine Surface. *Phys. Chem. Chem. Phys.* **2018**, *20* (40), 25812−25821.
(49) Qiu, Z.; Tang, D.; Shu, J.; Chen, G.; Tang, D. Enzyme-Triggered Formation of Enzyme-Tyramine Concatamers on Nanogold-Functionalized Dendrimer for Impedimetric Detection of Hg(II) with Sensitivity Enhancement. *Biosens Bioelectron* **2016**, *75*, 108−115.
(50) Xu, M.; Gao, Z.; Wei, Q.; Chen, G.; Tang, D. Hemin/G-Quadruplex-Based DNAzyme Concatamers for in Situ Amplified Impedimetric Sensing of Copper(II) Ion Coupling with DNAzyme-Catalyzed Precipitation Strategy. *Biosens Bioelectron* **2015**, *74*, 1−7.
(51) Zeng, R.; Xu, J.; Liang, T.; Li, M.; Tang, D. Photocurrent-Polarity-Switching Photoelectrochemical Biosensor for Switching Spatial Distance Electroactive Tags. *ACS Sens* **2023**, *8* (1), 317−325.

https://doi.org/10.1021/acsomega.3c07856
ACS Omega 2024, 9, 1454−1462